Transition states and minimum energy pathways for the collapse of carbon nanotubes

Sulin Zhang,* Roopam Khare, and Ted Belytschko[†]

Department of Mechanical Engineering, Northwestern University, 2145 Sheridan Road, Evanston, Illinois 60208-3111, USA

K. Jimmy Hsia

Department of Mechanical and Industrial Engineering, University of Illinois, Urbana, Illinois 60801, USA

Steven L. Mielke and George C. Schatz

Department of Chemistry, Northwestern University, 2145 Sheridan Road, Evanston, Illinois 60208-3113, USA

Carbon nanotubes (CNTs) can undergo collapse from their customary cylindrical configurations to ribbons. The energy minima corresponding to these two states are identified using either atomistic molecular mechanics or the theory of finite crystal elasticity with reduced dimensionality. The minimum energy path between these two minima is found using the nudged elastic band reaction-pathway sampling scheme. The energetics of CNT collapse is explored for both single- and multi-walled CNTs as well as small bundles. The process has a strong diameter dependence, with collapse being more favorable for the larger diameter tubes, but is nearly independent of chirality. The saddle point always lies close to the collapsed state, and the absolute barrier energies—even for fairly short tube lengths—are sufficiently high, even when the reaction is highly exothermic, that thermal activation cannot initiate collapse via this pathway. The hydrostatic pressure required to buckle and collapse CNTs of various diameters is discussed.

I. INTRODUCTION

Both single-walled (SW) and multi-walled (MW) carbon nanotubes (CNTs) may undergo collapse to ribbon structures due to a variety of circumstances including the presence of impurities in the synthesis,[1] electron bombardment,[2,3] compression,[4] crushing in diamond anvils,[5] mechanical strain,[6] and hydrostatic pressure.[7–15] Collapsed MWCNTs have been observed by transmission electron microscopy[6,16–19] and by atomic force microscopy.[20–22] Conversion to ribbons significantly alters the mechanical, thermal, and electronic properties of CNTs and can thus affect their usefulness for applications. The collapse of CNTs has been extensively studied by continuum mechanics based methods and atomistic simulations.[11,17,20,23–34] In particular, Goddard and co-workers[24,25] considered the relative energetics of the cylindrical and collapsed structures of SWCNTs and outlined three stability regimes characterized by two threshold values of the tube diameter, d_1 and d_2. For SWCNTs with diameter $d < d_1$, only the cylindrical configuration is stable; for $d_1 < d < d_2$, the cylindrical configuration is energetically favorable, while the collapsed configuration is metastable; for $d > d_2$, the collapsed configuration is energetically favorable, while the cylindrical configuration is only metastable. In the work presented here we extend such analyses to MWCNTs and bundles. We also determine the saddle points and minimum energy paths connecting the cylindrical and collapsed configurations. This information is used to estimate the magnitude of the hydrostatic pressure that is sufficient to initiate buckling and collapse.

II. METHODOLOGY

For the present set of calculations, we adopt the second-generation Tersoff-Brenner potential[35] and a Lennard-Jones (LJ) potential with the parameters of Girifalco *et al.*[36] to describe the short-ranged covalent interactions and the long-ranged nonbonded interactions in CNTs, respectively. Registry effects[17,37,38] are not well modeled by such simple interaction potentials. It has been suggested that such effects can stabilize locally twisted free-standing MWCNT ribbons;[17,38] to accurately incorporate registry effects, a simulation model that utilizes a registry-dependent potential[37] may be required. In calculating the nonbonded interaction energy, interatomic distances below a radius of 3.0 Å are excluded so that the accuracy of the covalent interactions is not affected. We also neglect nonbonded interactions for interatomic distances greater than 9.6275 Å and shift the LJ potential upward by a linear function determined by the requirement that the energy and force vanish at the cutoff distance. All calculations employed periodic boundary conditions in the axial direction.

Most of the results were obtained via direct atomistic molecular mechanics calculations. For a few of the largest calculations, in order to reduce the number of degrees of freedom, the atomistic models were coarse-grained by finite elements based on a theory of finite elasticity for crystalline monolayers.[39] This theory overcomes the drawbacks of the standard Cauchy-Born rule in treating atomic monolayers, and establishes the strain energy density function for graphene structures using exponential maps. This method significantly reduces computational cost, while remaining faithful to the corresponding atomistic model for defect-free, homogeneously deformed CNTs.[40] For the present study we also assume uniform deformation along the tube axis (i.e., a plane-strain condition); this assumption further reduces the number of degrees of freedom of the system. Following the exponential Cauchy-Born rule, the strain-energy density function W can be cast in terms of the interaction potentials.[39,40] Given a deformation map ϕ the total energy

in the system is then the sum of the elastic strain energy Π_{cv} and the nonbonded potential Π_{nb}

$$\Pi(\phi) = \Pi_{cv} + \Pi_{nb} = \int_{\Omega_0} W[\mathbf{C}(\phi); \mathbf{k}(\phi)] d\Omega_0$$
$$+ \frac{2}{S_0^2} \int_{\Omega_0} \int_{\Omega_0} V_{nb}[\|\phi(\mathbf{X}) - \phi(\mathbf{Y})\|] d\Omega_{0\mathbf{Y}} d\Omega_{0\mathbf{X}},$$

(1)

where ϕ is the deformation map, S_0 is the area of the unit cell, W is the strain energy density, which is a function of the Cauchy-Green deformation tensor $\mathbf{C}$ and the normal curvature in the circumferential direction $\mathbf{k}$, and $\mathbf{X}$ and $\mathbf{Y}$ are material coordinates in the initial configurations.

We first obtain the cylindrical minimum configuration by using a limited memory BFGS geometry optimization algorithm.[41] To determine the collapsed configuration, the cylindrical configuration is deformed by prescribing displacements to selected nodes. At each step, the configuration of the tube is optimized for the given displacement constraints. As the interwall distance reaches ~3.4 Å (the interlayer separation distance in graphite), all the nodes are released, followed by a full relaxation. This procedure is also effective in finding the collapsed configurations for MWCNTs and CNT bundles. For SWCNTs, a good initial guess for the collapsed configuration is obtained by mapping the cylindrical configuration to a deformed configuration by

$$x = X(1 + \alpha|\cos\theta|); \quad y = Y(1 - \alpha|\sin\theta|),$$

(2)

where the wall separation depends on the parameter α, X and Y are the Cartesian coordinates orthogonal to the tube axis in the cylindrical configuration, x and y are the Cartesian coordinates orthogonal to the tube axis in the collapsed configuration, and θ is the polar angle of the point (X, Y). This deformation map transforms the cylindrical configuration to a dumbell-shaped configuration that is then fully relaxed, leading to the optimized collapsed configuration. The final collapsed configuration is independent of the deformation path from the cylindrical configuration. For small-diameter tubes, this deformed configuration bounces back to the original cylindrical configuration, indicating that a second local energy minimum, which corresponds to a collapsed configuration, does not exist.

After identifying the cylindrical and collapsed configurations, the nudged elastic band (NEB) algorithm[42] is employed to determine the MEP between these two local energy minima. The elastic band is discretized with 20 replicas that connect the two end states and the spring constants at each replica are carefully chosen to eliminate the sliding-down problem. We thus obtain the activation energy as well as a detailed view of the collapse process.

III. RESULTS AND DISCUSSION

Figures 1(a) and 1(b) show the cylindrical and collapsed configurations of a [40,0] nanotube. Figure 2(a) shows the relative energy difference $E_{cylindrical} - E_{collapsed}$ per unit area, between the cylindrical and collapsed configurations for a series of zigzag, [n,0], SWCNTs where n ranges from 10 to 200, and a series of armchair [m,m] SWCNTs where m ranges from 5 to 120. It is useful to remember that the diameter of an [n,m] SWCNT is given approximately by

$$d \approx 0.783 \sqrt{n^2 + nm + m^2} \text{ Å}.$$

(3)

For SWCNTs with small diameters, the collapsed configuration is not stable, so ΔE is not defined. Three stability regimes can be identified in terms of the tube diameter d. In region I ($d < d_1 \approx 24.2$ Å), only the cylindrical configuration is stable; in region II ($d_1 < d < d_2 \approx 62.4$ Å) where $\Delta E < 0$, the cylindrical configuration is energetically more stable, and the collapsed configuration is metastable; in region III ($d > d_2$) where $\Delta E > 0$, the collapsed configuration is energetically more stable, while the cylindrical configuration is at most metastable. (Note that the quoted d_1 and d_2 values refer to the diameters of the largest and smallest CNTs, respectively, that are not included in region II, from among the chiralities studied.) The second region contains zigzag tubes in the range $n = 32$ to 79, and armchair tubes in the range $m = 18$ to 45. We note that these d_1 and d_2 values are in reasonable agreement with the values ($d_1 \approx 22$ Å and $d_2 \approx 60$ Å) obtained by the atomistic study of Gao *et al.*[24] whereas the values ($d_1 = 13.98$ Å and $d_2 = 19.52$ Å) of Tang *et al.*,[32] obtained using an analytical continuum analysis, are significantly lower. The energy difference between the cylindrical and collapsed configurations for zigzag tubes is almost identical to that of armchair tubes of similar diameter, indicating that the relative energetics are nearly independent of tube chirality. Figure 2(b) shows the relative energy difference $E_{cylindrical} - E_{collapsed}$ per unit area as a function of the inner tube diameter for a series of double walled CNTs, where the tubes are of the form [n,n]/[$n+5$,$n+5$] and start with $n = 20$. For these double-walled CNTs the threshold tube diameter values d_1 and d_2 are larger than those for SWCNTs with $d_1 \approx 27.1$ Å and $d_2 \approx 80.0$ Å. Figure 1(c) and 1(d) show the cylindrical and collapsed configurations of a [30,30]/[35,35] double-walled CNT, respectively.

The strain energy increases with the number of shells for MWCNTs undergoing collapse since all of the walls deform; however, the change in surface energy during collapse remains relatively constant with increasing number of walls since the wall spacing changes significantly only for the inner-most shell. In Fig. 3, we examine the energy difference between the cylindrical and the collapsed configurations for a series of MWCNTs, with the number of walls ranging from 1 to 9. The indices of the shells are [$40+5n$,$40+5n$]($n = 0, 1, 2, \ldots, 8$), which ensures that the intershell spacing is roughly 3.4 Å. For all of these tubes, the collapsed configurations are metastable. As expected, ΔE monotonically decreases with increasing number of shells.

A CNT can be considered to result from the rolling of a graphene sheet with a particular rolling direction and circumference. Some strain energy is stored in CNTs due to the curvature introduced by this rolling; this energy is inversely proportional to the tube radius. During the transition from the cylindrical to the collapsed configuration, parts of the tube walls are flattened, which reduces the strain energy in
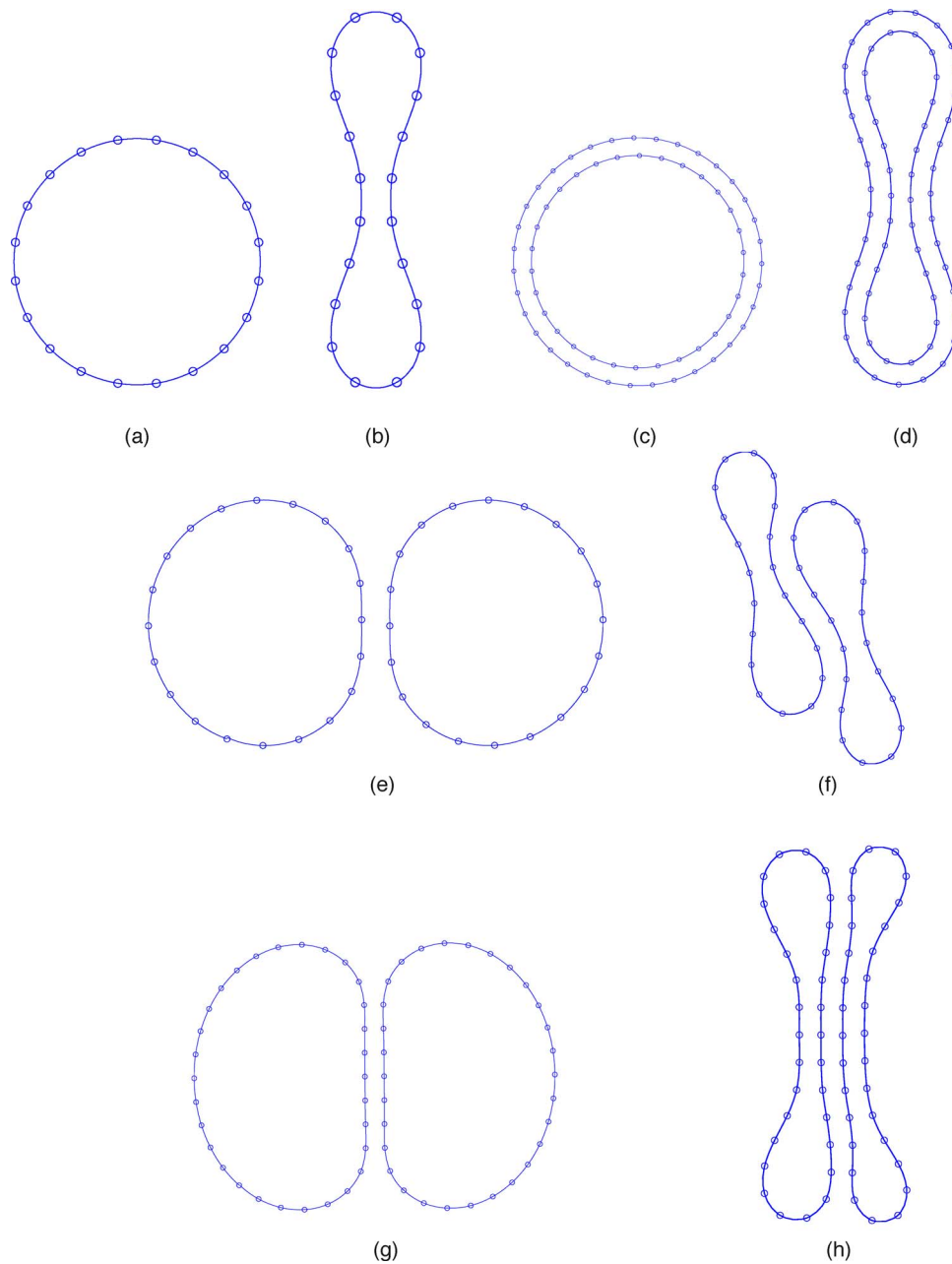
FIG. 1. (Color online) Fully relaxed cylindrical and collapsed configurations of CNTs. (a) [40,0] SWCNT, cylindrical configuration. (b) [40,0] SWCNT, collapsed configuration. (c) [30,30]/[35,35] double-walled CNT, cylindrical configuration. (d) [30,30]/[35,35] double-walled CNT, collapsed configuration. (e) Two [20,20] CNTs, original configuration. (f) Two [20,20] CNTs, collapsed configuration. (g) Two [30,30] CNTs, original configuration. (h) Two [30,30] CNTs, collapsed configuration.

these regions, and two semicircular edges, which have an almost constant radius (around 11 Å) independent of the initial radius of the tube, develop. The strain energy increase due to the formation of the ribbon edges is roughly independent of the tube diameter and exceeds the strain energy released by the flattening sections; thus, the total energy rises at the start of collapse. The attractive nonbonded interactions increase in magnitude as the walls of a CNT are brought closer together, and reach a maximum magnitude when the interwall spacing approaches ∼3.4 Å. The optimal change in the nonbonded interactions increases approximately linearly with the tube radius, and thus for large tubes this term easily

exceeds the strain energy. However, the CNT must be considerably distorted from the cylindrical configuration before the interwall spacing drops enough for a significant increase in the van der Waals interactions, so even for large tubes a substantial barrier can be expected.

For CNT bundles, the intertube van der Waals forces result in a flattening of the regions where the tubes are in contact. As a result, the initial relaxed configuration is not of cylindrical shape, as shown in Fig. 1(e) for a two [20,20] nanotube bundle and in Fig. 1(g) for a two [30,30] tube bundle. The intertube adhesion in bundles makes collapsed configurations substantially more stable than for the corre-

(a)

(b)

(c)
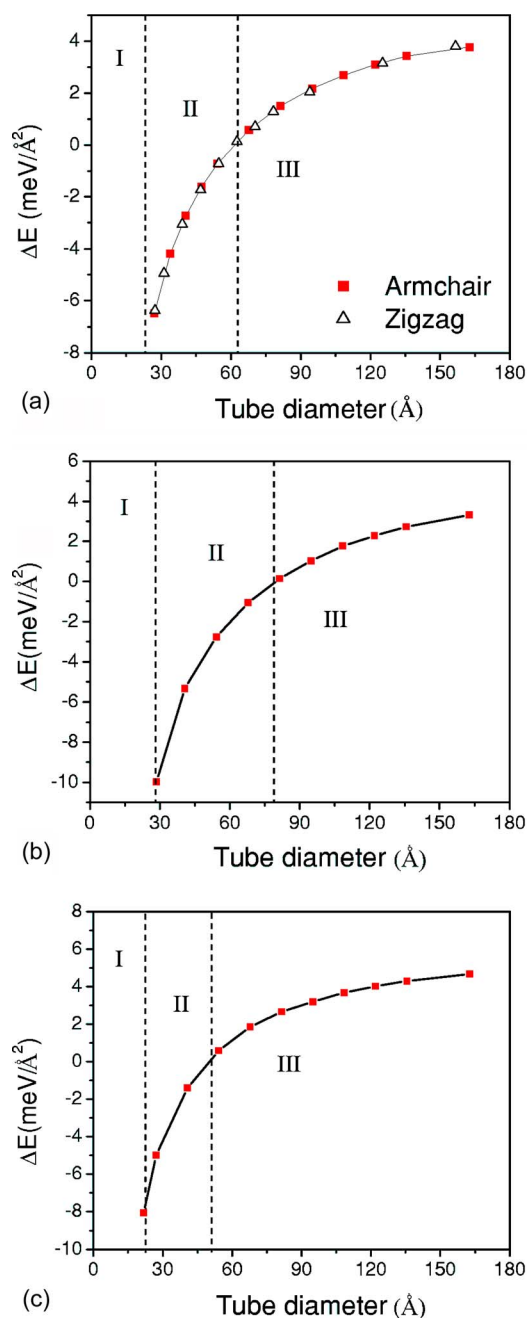
FIG. 2. (Color online) (a) Energy difference $\Delta E = E_{\text{cylindrical}} - E_{\text{collapsed}}$ per unit area between the cylindrical and the collapsed configurations for SWCNTs vs tube diameter. (b) As in (a) except for double-walled CNTs of the form $[n,n]/[n+5,n+5]$; the diameter refers to that of the inner tube. (c) As in (a) except for two-tube bundles, where the tubes are the same size, and the diameter values refer to that of a single tube.

sponding isolated SWCNTs. For example, in a [20,20] SWCNT, the collapsed configuration is not stable, while a collapsed equilibrium configuration for a two-tube [20,20] bundle can be found [Fig. 1(f)]. Thus, for two-tube bundles, the threshold values, d_1 and d_2, are shifted to smaller values as compared to isolated SWCNTs. Figure 2(c) displays the relative energetics for two-bundles consisting of a pair of identical armchair CNTs; our calculations show that d_1
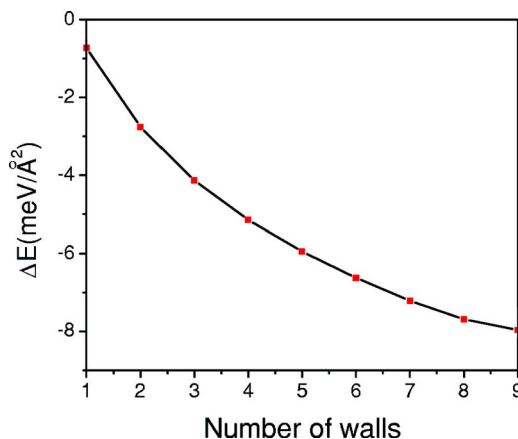
FIG. 3. (Color online) Energy difference $\Delta E = E_{\text{cylindrical}} - E_{\text{collapsed}}$ per unit area (of the inner shell) as a function of the number of walls. The shells are $[40+5n, 40+5n]$ for $n=0, 1, \ldots, 8$.

≈ 20.3 Å and $d_2 \approx 50.2$ Å. For a two-tube [20,20] bundle, the nanotubes slide with respect to each other along their contacting faces, forming a collapsed configuration that minimizes the surface energy, as shown in Fig. 1(f), while for the two-tube [30,30] bundle, and larger diameter two-tube bundles, the collapsed configuration remains approximately symmetric, as illustrated in Fig. 1(h). We expect that collapsed configurations will be further stabilized as the number of tubes in the bundle increases. Molecular dynamics calculations on SWCNTs in large bundles by Elliot *et al.*[11] indicate that tubes with diameters somewhere within the range of 42 to 69 Å are sufficiently large that they collapse spontaneously under atmospheric pressure.

We next used the NEB algorithm to determine the activation barrier and the MEP for CNT collapse. Figure 4 displays MEPs for the collapse of [60,0], [70,0], and [90,0] SWCNTs. Figure 5 displays cross sections at several representative
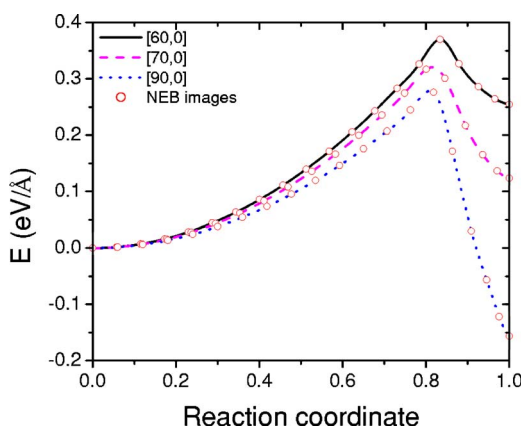
FIG. 4. (Color online) MEPs for the collapse of selected CNTs. The zeros of energy are relative to the cylindrical configurations and the energies are per unit length. The reaction coordinate is calculated as the Euclidean distance between a given configuration and the initial (cylindrical) configuration divided by the distance between the final (collapsed) and initial configuration. The symbols represent the images from the nudged elastic band calculation and the curves are cubic spline fits.
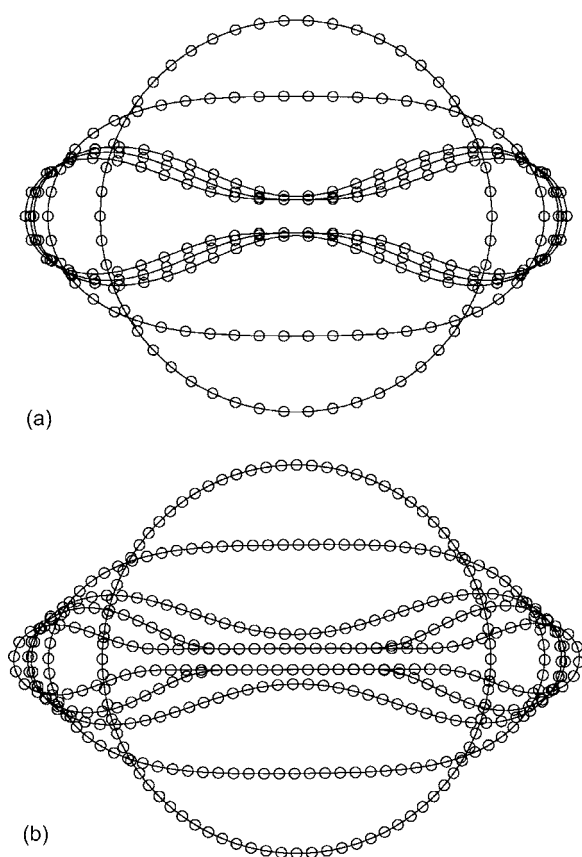
FIG. 5. (a) Cross sections for five configurations along the MEP for the collapse of a [50,0] CNT; configurations include the initial (cylindrical) configuration, the saddle point, the collapsed configuration, a configuration midway between the initial configuration and the saddle point, and a configuration midway between the saddle point and the final configuration. (b) Same as (a) except for an [80,0] CNT.

points along the MEP for the collapse of [50,0] and [80,0] SWCNTs. Figure 6 shows the dependence of the barrier height (per unit length) on the tube diameter for SWCNTs. The transition state always occurs fairly late along the reaction path and closely resembles the collapsed configuration, even for highly exothermic reactions (which is in contrast
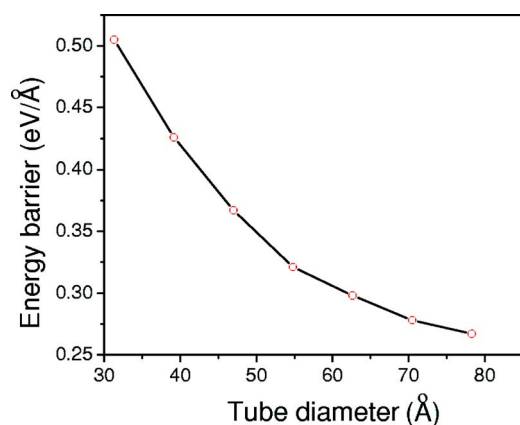
FIG. 6. (Color online) Activation energy barrier per unit length as a function of the tube diameter for the collapse of SWCNTs.

with typical behavior for exothermic reactions as predicted by Hammond's postulate). This occurs because the sidewalls must approach each other fairly closely before the attractive van der Waals interactions change significantly. Since the transition state occurs so late, much of the increased strain energy resulting from the formation of the ribbon edges has already been incurred; thus, the absolute barrier heights are quite high over a wide range of initial diameter values and are proportional to the length of the tube. This means that, except for unphysically short tubes, CNT collapse cannot proceed via this pathway by thermal activation. (For a 12.78 Å segment of a [60, 0] CNT the thermal rate constant for collapse at a temperature of 300 K is $O(10^{-80} \text{ s}^{-1})$.) Therefore, the experimentally observed collapsed CNT configurations are most likely due to mechanical processes. Since the energy barriers per unit length decrease monotonically with increasing tube diameter, the larger tubes will be easier to collapse by such means.

One widely studied CNT collapse mechanism involves the application of hydrostatic pressure.[7–15,23,26,28–34] Two regimes can be considered, the initial buckling as the system departs from perfectly circular cross sections and then the subsequent evolution of the system, which involves passage over a barrier similar to the one present in the MEP. Continuum elasticity[43] estimates of the buckling pressure, which were originally applied to CNT collapse by Yakobson *et al.*,[23] can be obtained via

$$P_b = \frac{2Y}{(1-\nu^2)}\left(\frac{h}{d}\right)^3, \tag{4}$$

where Y is the Young's modulus, h is the CNT shell-thickness parameter, and ν is Poisson's ratio. The shell thickness of a CNT is a nebulous quantity, and the use of the conventional value for h of 3.4 Å (which is chosen so that the Young's modulus of a CNT approximately matches the 1 TPa value of graphite) in Eq. (4), would lead to erroneously high results. Yakobson *et al.*[23] recommended parameter values of $Y=5500$ GPa, $h=0.66$ Å, and $\nu=0.19$, for use with Eq. (4), based on consistency with elasticity theory and a first generation Tersoff-Brenner reactive bond-order potential.[44] Equation (4) can be rewritten as

$$P_b = 24D/d^3, \tag{5}$$

where the flexural rigidity D is given as

$$D = \frac{Yh^3}{12(1-\nu^2)}. \tag{6}$$

Within a continuum approximation, the flexural rigidity can be related to the rolling energy per unit area E_R of a graphene sheet, via

$$E_R = \frac{D}{2R^2}, \tag{7}$$

so D, and hence P_b, can be obtained without specification of a shell thickness parameter. The parameters recommended by Yakobson *et al.*[23] correspond to $D=0.853$ eV; we obtain a value of $D=1.38$ eV, appropriate for the newer potential used here, by fitting to Eq. (7) the energies of the set of six

TABLE I. Comparison of buckling pressures P_b predicted from the theory of elasticity, with buckling onset pressures P_o and collapse pressures P_c predicted from Eq. (8) and the MEP data. The pressures are in units of GPa.

CNT	Diameter (Å)	P_b	P_o	P_c
[40,0]	31.3	1.73×10^{-1}	1.55×10^{-1}	2.5×10^{-1}
[50,0]	39.2	8.84×10^{-2}	8.73×10^{-2}	1.2×10^{-1}
[60,0]	47.0	5.12×10^{-2}	5.08×10^{-2}	7.3×10^{-2}
[70,0]	54.8	3.22×10^{-2}	3.21×10^{-2}	5.5×10^{-2}
[80,0]	62.6	2.16×10^{-2}	2.15×10^{-2}	3.1×10^{-2}
[90,0]	70.5	1.52×10^{-2}	1.53×10^{-2}	2.1×10^{-2}

zigzag CNTs for which we have calculated MEPs.

If the hydrostatic pressure is increased at a rate that is gradual enough for efficient energy redistribution to occur, we can expect the evolution of the CNT collapse process to closely resemble passage along the MEP; the exact path followed will depend on the pressure, but for pressures of reasonable magnitude we expect such differences to be small. If we approximate the true collapse path by the MEP, then the magnitude of the pressure required to collapse an isolated SWCNT needs to be high enough that

$$\frac{PA}{\sqrt{N}}(\hat{n} \cdot \hat{s}) > \nabla E \cdot \hat{s} \quad (8)$$

at every point along the reaction path, where P is the pressure (for hydrostatic pressure this acts normal to the CNT surface), E is the energy, $\hat{s}$ is a unit vector that points along the reaction path and toward collapse, $\hat{n}$ is an outward pointing unit normal vector, N is the number of atoms, and A is the area of the tube. We will associate the maximum pressure required by Eq. (8) with the collapse pressure P_c and we will also consider the onset pressure P_o required to begin motion along the MEP. These two pressures are compared to the buckling pressure predicted by elasticity theory in Table I for a series of zigzag CNTs. The continuum elasticity buckling pressures agree extremely well with the MEP motion onset pressures except for the smallest tube (where P_o was about 10% lower than P_b). The predicted collapse pressures are all about 40% higher than the continuum buckling pressures. These results are consistent with molecular dynamics simulations of the collapse of a [10,10] SWCNT (using a first generation Brenner potential) by Sun *et al.*,[31] where the observed buckling pressure was about 20% below the elasticity buckling prediction and full collapse occurred at a pressure that was about 50% about that of the elasticity buckling prediction.

For the largest CNT for which we have calculated an MEP, [90, 0], a pressure of about 150 atm is required to collapse the tube (note that 1 atm is $\sim 1.013 \times 10^{-4}$ GPa). The elasticity expression of Eq. (5) estimates a minimum diameter value for collapse at 1 atm of $\sim$370 Å. SWCNTs in bundles will collapse at much lower values; Elliot *et al.*[11] estimated a diameter between 42 and 69 Å for collapse at atmospheric pressure in large bundles. Bending and other stresses incurred during processing, purification, and handling may be expected to initiate collapse of large-diameter isolated SWCNTs by other mechanisms than those considered here. Thus, metastable cylindrical configurations of large-diameter tubes that are stable against pressure-induced collapse are still likely to be rare.

IV. CONCLUDING REMARKS

We have outlined three stability regimes for the relative stability of cylindrical and collapsed configurations of CNTs. For SWCNTs with diameters less than $\sim$24.2 Å, only cylindrical configurations are stable; for CNTs with diameters greater than $\sim$24.2 Å but less than $\sim$62.4 Å, equilibrium configurations have been found for both cylindrical and collapsed configurations, but the cylindrical configuration is energetically favorable; for diameters greater than $\sim$62.4 Å, the collapsed configuration is a lower energy configuration. We found that these characteristics are approximately independent of tube chirality. For MWCNTs these critical diameters have higher values, whereas for SWCNT bundles lower critical values are observed.

Using the nudged elastic band algorithm, we determined the MEP between the cylindrical and collapsed states. It was found that the transition state barrier heights decrease monotonically with increasing tube diameter. Nevertheless, these barriers, for all but the shortest of tube lengths, are sufficiently high that rates for thermal activation of CNT collapse via this pathway are always negligible. Lower barrier heights do, however, indicate that mechanical mechanisms for flattening CNTs will be more important for the larger radius tubes. The data along the MEP were also used to estimate hydrostatic pressure values that would initiate CNT buckling and collapse; the buckling values obtained agreed well with predictions of elasticity theory, and the predicted collapse pressures are about 40% higher than the buckling pressures.

*Present address: Department of Mechanical Engineering, University of Arkansas, Fayetteville, AR 72701, USA. Email address: szhang1@uark.edu

†Email address: tedbelytschko@northwestern.edu

[1] W. Qian, F. Wei, T. Liu, and Z. Wang, J. Chem. Phys. **118**, 878 (2003).

[2] N. G. Chopra, F. M. Ross, and A. Zettl, Chem. Phys. Lett. **256**, 241 (1996).

[3] V. H. Crespi, N. G. Chopra, M. L. Cohen, A. Zettl, and S. G. Louie, Phys. Rev. B **54**, 5927 (1996).

[4] O. Lourie, D. M. Cox, and H. D. Wagner, Phys. Rev. Lett. **81**, 1638 (1998).

[5] Z. Wang, J. Phys. Chem. B **108**, 18192 (2004).

[6] M.-F. Yu, O. Lourie, M. J. Dyer, K. Moloni, T. F. Kelly, and R. S. Ruoff, Science **287**, 637 (2000).

[7] J. R. Wood, M. D. Frogley, E. R. Meurs, A. D. Prins, T. Peijs, D. J. Dunstan, and H. D. Wagner, J. Phys. Chem. B **103**, 10388 (1999).

[8] J. Tang, L.-C. Qin, T. Sasaki, M. Yudasaka, A. Matsushita, and S. Iijima, Phys. Rev. Lett. **85**, 1887 (2000).

[9] M. J. Peters, L. E. McNeil, J. P. Lu, and D. Kahn, Phys. Rev. B **61**, 5939 (2000).

[10] J. Tang, L.-C. Qin, T. Sasaki, M. Yudasaka, A. Matsushita, and S. Iijima, J. Phys.: Condens. Matter **14**, 10575 (2002).

[11] J. A. Elliott, J. K. W. Sandler, A. H. Windle, R. J. Young, and M. S. P. Shaffer, Phys. Rev. Lett. **92**, 095501 (2004).

[12] P. Puech, H. Hubel, D. J. Dunstan, A. Bassil, R. Bacsa, A. Peigney, E. Flahaut, C. Laurent, and W. S. Bacsa, Phys. Status Solidi B **241**, 3360 (2004).

[13] R. B. Capaz, C. D. Spataru, P. Tangney, M. L. Cohen, and S. G. Louie, Phys. Status Solidi B **241**, 3352 (2004).

[14] M. Monteverde and M. Nunez-Regueiro, Phys. Rev. Lett. **94**, 235501 (2005).

[15] M. S. Amer, M. M. El-Ashry, and J. F. Maguire, J. Chem. Phys. **121**, 2752 (2004).

[16] N. G. Chopra, L. X. Benedict, V. H. Crespi, M. L. Cohen, S. G. Louie, and A. Zettl, Nature (London) **377**, 135 (1995).

[17] M.-F. Yu, M. J. Dyer, J. Chen, D. Qian, W. K. Liu, and R. S. Ruoff, Phys. Rev. B **64**, 241403(R) (2001).

[18] L. N. Bourgeois and L. A. Bursill, Chem. Phys. Lett. **277**, 571 (1997).

[19] S. Liu, J. Yue, and R. J. Wehmschulte, Nano Lett. **2**, 1439 (2002).

[20] L. X. Benedict, N. G. Chopra, M. L. Cohen, A. Zettl, S. G. Louie, and V. H. Crespi, Chem. Phys. Lett. **286**, 490 (1998).

[21] M.-F. Yu, T. Kowalewski, and R. S. Ruoff, Phys. Rev. Lett. **86**, 87 (2001).

[22] M.-F. Yu, M. J. Dyer, and R. S. Ruoff, J. Appl. Phys. **89**, 4554 (2001).

[23] B. I. Yakobson, C. J. Brabec, and J. Bernholc, Phys. Rev. Lett. **76**, 2511 (1996).

[24] G. Gao, T. Cagin, and W. A. Goddard III, Nanotechnology **9**, 184 (1998).

[25] J. Che, T. Cagin, and W. A. Goddard III, Theor. Chem. Acc. **102**, 346 (1999).

[26] P. E. Lammert, P. Zhang, and V. H. Crespi, Phys. Rev. Lett. **84**, 2453 (2000).

[27] M. Arroyo and T. Belytschko, Mech. Mater. **35**, 193 (2003).

[28] S.-P. Chan, W.-L. Yim, X. G. Gong, and Z.-F. Liu, Phys. Rev. B **68**, 075404 (2003).

[29] A. Pantano, D. M. Parks, and M. C. Boyce, J. Mech. Phys. Solids **52**, 789 (2004).

[30] H. J. Liu and K. Cho, Appl. Phys. Lett. **85**, 807 (2004).

[31] D. Y. Sun, D. J. Shu, M. Ji, F. Liu, M. Wang, and X. G. Gong, Phys. Rev. B **70**, 165417 (2004).

[32] T. Tang, A. Jagota, C.-Y. Hui, and N. J. Glassmaker, J. Appl. Phys. **97**, 074310 (2005).

[33] H.-S. Shen, Int. J. Solids Struct. **41**, 2643 (2004).

[34] X. Ye, D. Y. Sun, and X. G. Gong, Phys. Rev. B **72**, 035454 (2005).

[35] D. W. Brenner, O. A. Shenderova, J. A. Harrison, S. J. Stuart, B. Ni, and S. B. Sinnott, J. Phys.: Condens. Matter **14**, 783 (2002).

[36] L. A. Girifalco, M. Hodak, and R. S. Lee, Phys. Rev. B **62**, 13104 (2000).

[37] A. N. Kolmogorov and V. H. Crespi, Phys. Rev. Lett. **85**, 4727 (2000).

[38] B. Liu, M.-F. Yu, and Y. Huang, Phys. Rev. B **70**, 161402(R) (2004).

[39] M. Arroyo and T. Belytschko, Phys. Rev. B **69**, 115415 (2004).

[40] S. Zhang, S. L. Mielke, R. Khare, D. Troya, R. S. Ruoff, G. C. Schatz, and T. Belytschko, Phys. Rev. B **71**, 115403 (2005).

[41] R. H. Byrd, P. Lu, and J. Nocedal, SIAM J. Sci. Comput. (USA) **16**, 1190 (1995).

[42] H. Jonsson, G. Mills, and K. W. Jacobsen, in *Classical and Quantum Dynamics in Condensed Phase Simulations*, edited by B. J. Berne, G. Ciccotti, and D. F. Coker (World Scientific, Singapore, 1998), p. 385.

[43] S. Timoshenko, *Theory of Elastic Stability* (McGraw-Hill, New York, 1936).

[44] D. W. Brenner, Phys. Rev. B **42**, 9458 (1990); **46**, 1948(E) (1992).